Southwestward growth of plateau surfaces in eastern Tibet

Kai Cao (kai.cao@cug.edu.cn)
China University of Geosciences https://orcid.org/0000-0002-1272-8758

Anne Replumaz
Université Grenoble Alpes

Yuntao Tian
Sun Yat-sen University

Laurent Husson
Grenoble

Guo-can Wang
China University of Geosciences

Tianyi Shen
China University of Geosciences

Peter Reiners
University of Arizona

Matthias Bernet
ISTerre, University Grenoble Alpes

Peter van der Beek
Université Grenoble Alpes, Potsdam University

Article

Keywords: Tibetan Plateau, Orogeny, Landscape evolution, Low-relief surfaces, Thermochronology

Posted Date: October 16th, 2020

DOI: https://doi.org/10.21203/rs.3.rs-89539/v1

Southwestward growth of plateau surfaces in eastern Tibet

Kai Cao [1, 2]*, Anne Replumaz [3], Yuntao Tian [4], Laurent Husson [3], Guocan Wang [1, 2], Tianyi Shen [1], Peter Reiners [5], Matthias Bernet [3], Peter van der Beek [3,6]

[1] Hubei Key laboratory of Critical Zone Evolution, School of Earth Sciences, China University of Geosciences, Wuhan 430074, China

[2] Center for Global Tectonics, State Key Laboratory of Geological Processes and Mineral Resources, China University of Geosciences, Wuhan 430074, China

[3] Institut des Sciences de la Terre (ISTerre), Université Grenoble Alpes, CNRS, CS 40700, Grenoble 38058, France

[4] Guangdong Provincial Key Lab of Geodynamics and Geohazards, School of Earth Sciences and Engineering, Sun Yat-sen University, Guangzhou, China

[5] Geoscience Department, University of Arizona, Tucson, Arizona, USA

[6] Institute of Geosciences, Potsdam University, 14476 Potsdam, Germany

*Kai Cao, **Email:** kai.cao@cug.edu.cn

Word count: 4829; Abstract: 182; Figures: 5; Appendixes: 10 items (2 figures, 8 tables); Refs: 76.

Abstract

Both the kinematics and dynamics for topographic growth of the Tibetan Plateau remain debated despite their significance for understanding the evolution of continental lithospheric geodynamics, climate, and biodiversity in Asia. Morphometric analysis reveals the continuity of high-elevated peneplains through the Songpan-Garze-Yidun, Qiangtang and Lhasa terranes in eastern Tibet. Inverse thermal-history modeling of thermochronological data indicates slow cooling of these terranes since 80-60 Ma, 40-35 Ma and 20-5 Ma, respectively, which is interpreted as marking tectonic and topographic stabilization of the plateau surfaces. The diachronous stabilization of flat plateau surfaces and early encroachment suggests decoupling of plateau surface formation from Neogene river incision and tectonics. This southwestward piecemeal expansion of small plateaus suggests that the high-elevation, low-relief landscape of eastern Tibet has been constructed during distinct orogenic episodes prior and during the early stages of India-Asia collision. A late stage of tectonic activity during Neogene only moderately remodeled the outer rims of the plateaus and the valleys that delineate the transcurrent faults, while lower crustal channel flow only leveled the distinct plateaus to a unique elevation, thereby triggering river incision in eastern Tibet.

Keywords

Tibetan Plateau; Orogeny; Landscape evolution; Low-relief surfaces; Thermochronology

Introduction

The Tibetan Plateau, with vast flat interiors and narrow steep margins (Fig. 1), is the highest and largest orogenic plateau on Earth and mainly rose in the aftermath of the India-Asia collision ca. 60-50 million years ago (Ma) [1,2]. The topographic evolution of the plateau remains debated and under-constrained, despite its significance for understanding the geodynamics of continental lithospheric deformation [3,4], the Asian monsoon system [5,6], and biodiversity evolution [7]. In particular, the origin of high-elevation, low-relief surfaces that are key elements of the Tibetan landscape has attracted growing attention in recent years but their geodynamic origin remains elusive [8-11]. Two end-member hypotheses have been proposed to explain the growth and flatness of the Tibetan topography: oblique crustal subduction accompanied by continental block extrusion [4,12] and lower crustal flow [3,13]. The former model predicts the Eocene rise of southern Tibet followed by the piecemeal uplift of central and northern Tibet, coeval with crustal shortening and magmatism related to lithosphere subduction from Oligocene to Pliocene. The flatness of this internally-drained area of the plateau is attributed to basin infill [4,9,14] and inferred to have formed prior to early Miocene [14]. In contrast, the latter hypothesis invokes topographic loading in the central plateau leading to eastward expansion of externally-drained, gentle plateau margins since the late Miocene. This model envisions the formation of low-relief plains close to sea level and surface uplift to high elevation in the later stage of the Tibetan orogeny [15,16].

Both hypotheses have recently been challenged by numerical simulations in which the low-relief surfaces in eastern Tibet may form in situ as a result of the low erosion power in drainage areas that become isolated due to tectonically-driven surface uplift and disruption of river patterns [11]. However, these model results were recently refuted by new landscape-evolution modelling, which support the evolution of a preexisting uplifted low-relief landscape incised by river networks [10]. The existence of such old landscape seems compatible with the development of low-relief surfaces at high elevations (>4000 m) in central, western and southeastern Tibet by or prior to the India-Asia collision (Fig. 1A), as indicated by stable-isotope paleoaltimetry and low-temperature thermochronometry [17-20]. A significant part of this ancient topography in central Tibet that was termed "Proto-Tibetan Plateau" [21] may be inherited from crustal shortening and thickening prior to the India-Asia collision [20,22].

Improved constraints on the timing of development of low-relief plateau surfaces at a larger spatial resolution are crucial to better understand the topographic and geodynamic evolution of the Tibetan Plateau. A common tool to estimate palaeoaltimetry are stable isotopes, which provide direct quantitative paleoelevation estimates of Cenozoic basins. However, they do not necessarily indicate the timing of plateau uplift at a regional scale. In addition, stable isotope paleoaltimetry relies largely on sampling of unaltered paleosoil and pedogenic carbonates in basin sediments having precise age control [23], which is challenging in terrestrial sediments [24]. The absolute age of the samples used for obtaining paleoelevation estimates thus only gives a lower bound on the timing of surface uplift, i.e. it is the most recent plausible age of uplift. The contrasting paleoelevation estimates derived from paleoaltimetry and paleontology in Tibet have been ascribed to potential uncertainties of paleogeography and topography variations as input for paleoelevation reconstructions based on stable isotopes [25]. Alternatively, low-temperature (e.g., zircon and apatite (U-Th)/He and apatite fission track) thermochronology cannot constrain paleoelevations, but can be used to infer the timing and magnitude of topographic relief change by deriving spatial-temporal patterns of exhumation rates as a result of erosional denudation and tectonic exhumation [26]. Thermochronological data are complementary to paleoaltimetry data, as they allow quantifying the thermal-tectonic histories of the plateau surfaces and are applied to constrain landscape evolution at a broader scale. In principle, the onset of extremely slow cooling and exhumation for the low-relief plateau surfaces rules out significant orogenic relief growth or erosion since then, and thus can be interpreted as recording the formation of relict landscapes preserved at high elevations (e.g., ref.[17]). Upon this hypothesis, we compiled new and published thermochronological data to reconstruct thermal histories of selected low-relief surfaces of different terranes in eastern Tibet to constrain the onset of topographic stabilization.

Results

Tectonic and geomorphologic features of eastern and southeastern Tibet

Eastern Tibet is a collage of major lithospheric fragments, including the Songpan-Garze, Yidun, Qiangtang, Lhasa and Himalaya terranes (Figs. 1A and 1B). This region has experienced a prolonged tectonic history of terrane accretion resulting from the closure of the Paleo-, Meso- and Neo-Tethys Oceans during Paleozoic-Mesozoic times [27]. Since the Cenozoic, extensive intra-continental deformation affected the area under the compound effects of India-Asia convergence and Pacific-Indonesia subduction [4,27].

The present topography of eastern Tibet is characterized by large areas of high-elevation, low-relief landscape that were interpreted as relict plateau surfaces [8] (Fig. 1B). In order to examine the topographic features of different terranes, we extracted a topographic swath profile from the Lhasa to Songpan-Garze terranes, crossing the Eastern Lhasa plateau (ELP), Zuogong plateau (ZGP), Markam-Weixi plateau (MKP-WP), Litang plateau (LTP) and Kangding plateau (KDP), which highlights the remarkable continuity of the plateau surfaces (Figs. 1C and 1D). The maximum elevations of the relict landscapes representative of plateau surfaces are ~4,600-4,800 m in the Kangding plateau and ~4,800-5,200 m in the Litang plateau, they drop to ~4,600 m in the Markam plateau, but increase abruptly to ~5,200-5,600 m in the Zuogong plateau and Eastern Lhasa plateau. These surfaces have been dissected by large rivers (i.e., Yalong River, Jinsha River, Lancang River and Nu River; Fig. 1B) and sliced by major strike-slip faults (e.g., Xianshuihe, Litang and Jiali faults; Figs. 1C and 1E) in Neogene times, as recorded by thermochronology and cosmogenic nuclide dating [15,28-33]. Relief is generally less than ~600 m across the plateau regions, with higher relief corresponding to the areas disrupted by river incision and strike-slip faulting (Figs. 1C and 1D). In the eastern Qiangtang terrane, smooth relict surfaces along the divide between the Jinsha River and Lancang River extend continuously from the Markam to the Deqin and Weixi plateaus, with maximum elevations decreasing from 4,600-5,000 m to 3,500-3,600 m (Figs. 1B and S1).

The topographic history of eastern and southeastern Tibet remains debated. Rapid incision of the Jinsha-Yangtze River, dated by low-temperature thermochronology, was used to infer the onset of widespread surface uplift in southeastern Tibet at ~13-9 Ma [15,28]. Despite the difference in incision histories of major rivers that were used to infer surface uplift (Fig. 1C), middle Miocene accelerated incision of the Lancang (Mekong) River has recently been interpreted to be related to the intensification of the Asian monsoon rather than plateau uplift [30]. Stable-isotope paleoaltimetry on Paleogene basin sediments suggest uplift of eastern and southeastern Tibet close to modern surface elevations of ~3-4 km above sea level (asl.) by the late Eocene [19,34-36] (Fig. 1D). However, other paleoelevation reconstructions yield much lower estimates of 1-3 km asl. [24,37,38] (Fig. 1B), implying an additional ~1-1.5 km of post-Eocene surface uplift [37]. Along the eastern and southeastern margins of the Tibetan Plateau, widespread rapid exhumation at ~30-20 Ma, as documented by thermochronological data, may be related to compressive deformation along the Longmen Shan and Yulong thrust belts, which would have created the local topographic relief [39,40]. Middle-late Miocene exhumation of the Longmen Shan has been interpreted to be related either to lower crustal flow [15,28] or to continued thrusting [40,41].

Thermal histories of the Zuogong, Markam and Weixi plateaus

In order to reconstruct the exhumation histories of selected plateau surfaces, we report new zircon and apatite (U-Th)/He (ZHe and AHe) and apatite fission-track (AFT) thermochronology data, in addition to zircon U-Pb geochronology data from 15 samples in the Zuogong, Markam and Weixi plateaus (Fig. 2; Table S1; Datasets S1-S4). The three low-temperature thermochronometric systems record cooling through a temperature window of ~220-40 °C [42]. In the Zuogong-Markam plateaus, 11 samples were collected at elevations between 4,300 m and 5,000 m on the plateau surfaces, as well as on the rim of the plateau cut by the Lancang River draining to the southeast. Samples from the late Triassic Zuogong batholith (Table S1) yield AFT ages ranging between 15 ± 2 Ma and 26 ± 3 Ma with mean track lengths between 14.2 ± 1.0 µm and 14.9 ± 0.8 µm (Fig. 2A; Table S1; Dataset S1). The youngest and oldest ages are from samples collected in the center and near the top of the batholith, respectively. The lower-temperature AHe weighted-mean ages overlap with their corresponding AFT ages within error and vary between 12.5 ± 0.9 Ma in the northern pluton and 28.7 ± 1.5 Ma on the western plateau rim, broadly consistent with 10 published single-grain AHe ages clustering at 18-20 Ma [43] (Fig. 2A; Table S1; Dataset S2). For the higher-temperature ZHe thermochronometer, weighted-mean ages from replicates vary from 37.0 ± 0.3 Ma for a sample collected on the northeast plateau rim to 60.2 ± 5.2 Ma on the eastern rim. In addition, one sample from Mesozoic sandstone of the Markam fold-and-thrust belt (Fig. 2A) yields an AFT age and an AHe weighted mean age of 76.3 ± 12.7 Ma and 41.3 ± 2.5 Ma, respectively. This new AFT age overlaps with a published AFT age of 70.9 ± 5.9 Ma [44] in the hanging wall of a thrust sheet east of Markam.

In the Weixi plateau, four samples were collected from the Triassic Ludian batholith at elevations between 2,360 m and 2,900 m on the plateau surface and along a tributary valley of the Jinsha River (Fig. 2B). AFT ages range between 61 ± 9 Ma and 118 ± 12 Ma, with mean track lengths between 13.9 ± 1.0 µm and 14.2 ± 1.1 µm, broadly consistent with existing AFT age and track-length data [44] (Fig. 2A; Tables S1; Dataset S1). For the higher-temperature ZHe system, the weighted-mean age for a sample collected near the top of the plateau is 117 ± 7 Ma, consistent with previous ZHe data [45]. Two AHe weighted-mean ages of 30.7 ± 1.3 and 62 ± 10 Ma are younger than their corresponding AFT and ZHe ages and overlap with previously published AHe ages in this region [45-47].

We modelled the cooling histories of rocks sampled from the low-relief surfaces of the Zuogong, Markam and Weixi plateaus, respectively (Fig. 2 and Fig. S2). For these samples we have multiple-thermochronometer data to perform inverse modeling, taking into account AFT ages, track-length distributions and Dpar, together with ZHe and AHe data (see Table S2 for modeling constraints). Modeling results from the Zuogong plateau show two episodes of rapid cooling at ca. 36-34 Ma and ca. 21-18 Ma, at rates of 30-40 °C/Myr, followed by a protracted period of extremely slow cooling at a rate of <0.5 °C/Myr (Fig. 2C). The best-fit thermal history of sample CD260 from the Markam plateau shows a phase of accelerated cooling between 40-30 Ma at a rate of ~3 °C/Myr, followed by slow cooling at a rate of <0.5 °C/Myr (Fig. 2D). In contrast, thermal histories from the Weixi plateau yield two rapid cooling episodes at ca. 90 Ma and 40-35 Ma, at rates of ~100 °C/Myr and ~16 °C/Myr respectively, followed by a protracted period of extremely slow cooling at a rate of <1 °C/Myr since the late Eocene (Fig. 2E). The Cretaceous rapid cooling occurred at several localities throughout the Qiangtang terrane [45,46]. Similarly, late Eocene rapid exhumation followed by slow cooling until present also occurred nearby in the hanging wall of the

Ludian-Zhonghejiang thrust to the west of the Jianchuan basin, suggesting late Eocene activity of the thrust belt and cessation thereafter [46]. Between 90-40 Ma, the sampled rocks experienced reheating, probably related to the deposition of Cretaceous-Eocene clastic sediments that are preserved nearby in the Jianchuan area [39]. Taken together, the cooling histories from the plateau surfaces of the Qiangtang terrane reveal widespread Eocene rapid cooling, followed by a late stage of accelerated cooling at ca. 20 Ma in the western part of the terrane. This pattern is consistent with southwestward younging AFT and AHe ages from the Markam-Weixi and Zuogong plateaus (Figs. 1C and S1). Assuming a paleo-geothermal gradient of 30 ± 5 °C/km, this yields average erosional exhumation rates of <0.014 mm/yr and 0.028 mm/yr for the samples in the Zuogong-Markam and Weixi plateaus, respectively, since the transition to slow cooling (Figs. 3C-E). These million-year-scale erosion rates roughly overlap with millennial-scale erosion rates of 0.02 ± 0.02 mm/yr, 0.03-0.04 mm/yr and 0.02-0.09 mm/yr for catchments draining the Zuogong [48], Litang [49] and Kangding [50] plateaus, respectively.

Discussion

Southwestward encroachment of low-relief plateau surfaces in eastern Tibet

[17]In eastern Tibet, the latest transition timing to protracted slow cooling that is inferred from thermal histories marks the onset ages of establishment of low-relief surfaces, evidenced by extremely low erosion rates at million- and millennial-year timescales affecting areas with low to moderate relief in each terrane (Fig. 3). In the Songpan-Garze-Yidun terranes, samples at high elevations (>4,000 m) and low relief (<600 m) regions in the Litang and Kangding plateau surfaces yield mainly Mesozoic to early Cenozoic (50-150 Ma) AHe and AFT cooling ages, indicating slow erosion rates of <0.05 mm/yr during the Cenozoic (Figs. 1D and 3A). Prolonged slow surface erosion, at rates of 0.01-0.03 mm/yr during the Cenozoic [15,51-53], in line with catchment-wide millennial erosion rates of <0.02-0.09 mm/yr [49,50] (Fig. 3), suggests that the low-relief landscapes in the Litang and Kangding plateaus were established before the India-Asia collision and maintained throughout most of the Cenozoic, consistent with little crustal thickening and exhumation [51]. The continuity of plateau surfaces with common formation ages suggests that a unifying flat landscape extended from the southern Songpan-Garze to the Yidun terranes by the early Cenozoic. The planation of

pre-Cenozoic summit relief was likely related to widespread tectonic denudation in the late Cretaceous-early Cenozoic, reflected by the youngest AFT and AHe peak ages of 60-80 Ma (Fig. 4C).

In the Qiangtang terrane, AHe and AFT ages cluster in the early-middle Cenozoic (31-65 Ma) for high elevation samples (>4,000 m) collected from low-relief (<600 m) regions of the Zuogong and Markam-Weixi plateaus (Fig. 1D), indicating slow erosion rates of <0.05 mm/yr (Fig. 3B). The low-relief surfaces in the northeastern Qiangtang apparently formed during the late Eocene at high elevations, as suggested by geological, thermochronological and paleoaltimetry evidence. Widespread exposure of flat-lying 34-36 Ma volcanic rocks [35] above an angular unconformity in the Markam plateau implies that the Markam fold-and-thrust belt was activated and exhumed to the surface before late Eocene volcanism (Figs. 2C and 2D). This episode of compressive deformation seemingly prevailed in the Qiangtang and Lhasa terranes, and was recorded at several other localities [20,45,46,54] (e.g., central Tibet, Zuogong, Weixi and Jianchuan; Fig. 1A), compatible with the youngest AHe and AFT age peaks of ca. 40 Ma throughout the plateau surfaces (Figs. 1D and 4B). Crustal thickening of the Qiangtang terrane was likely related to the India-Asia collision and resulted in surface uplift to elevations as high as today. Continuous slow exhumation in the Markam plateau since late Eocene times at a rate of <0.01 mm/yr indicates stabilization of low-relief surfaces during most of the Cenozoic (Fig. 2D), which precludes significant tectonically-driven denudation. The consistency of slow cooling rates for the Markam and Weixi plateaus (Figs. 2D and 2E) suggests the formation of a continuous smooth landscape that extended from Markam to Weixi by late Eocene, bypassing a remnant plateau surface at Deqin that has been dismembered by late Cenozoic faulting and river incision [55].

With respect to the northeastern Qiangtang terrane, the transition to slow denudation at ca. 20 Ma for the Zuogong plateau suggests stabilization of the flat surface at least 15-20 Myr later than for the Markam-Weixi plateaus in southwestern Qiangtang, as revealed by thermal-history modeling (Fig. 2C). Early-Miocene rapid cooling subsequent to late-Eocene rapid cooling suggests that the late-Eocene topography of the Zuogong plateau has been rejuvenated during the early Miocene. As the Markam plateau surface has been stabilized at ~4,600 m since late Eocene, given the Zuogong plateau surface yielded similar elevation of ~4,600 m after bulk Eocene crustal thickening of the Qiangtang block, it can be deduced that the present height of ~5,200 m of the Zougong plateau surface has possibly been achieved by tectonic uplift of at least 600 m with respect to its Eocene elevation at ~4,600 m since ca. 20 Ma.

In the easternmost Lhasa terrane, thermal-history modeling of zircon and apatite (U-Th)/He data from the eastern Lhasa plateau yield two stages of rapid cooling in early-Miocene and late-Miocene times [56], respectively. Early-Miocene rapid cooling is coeval with the latest tectonic activity in the southwestern Qiangtang terrane, whereas the younger episode of accelerated cooling suggests that the landscape of the eastern Lhasa plateau is homogeneous in morphology, but younger than the Zuogong plateau.

Collectively, our new thermochronological data together with existing data highlight the diachronous encroachment of plateau surfaces in the Songpan-Garze-Yidun, northeastern Qiangtang, southwestern Qiangtang and eastern Lhasa terranes, by the Late Cretaceous-Paleogene (~80-60 Ma), late Eocene (~45-35 Ma), early Miocene (~20 Ma) and late Miocene (~10-5 Ma), respectively in eastern Tibet (Fig. 4). The hilly relief that resulted from Mesozoic-early Cenozoic orogenesis could be rapidly reduced by erosion [57]. We thus suggest that the surface processes responsible for lowering high-relief ranges and infilling of adjacent lowlands may have also been responsible for the formation of low-relief plateau surfaces at high elevations in the northeastern Qiangtang terrane during early Cenozoic times. This interpretation is analogous to previous models for the presence of low-relief landscapes in central Tibet [4,9,14]. At least 3-5 km of syntectonic sediments were shed into the foreland basins (e.g., Sichuan, Xichang and Chuxiong basins; Figs. 1B and 4D) along the western South China block prior to the Cenozoic [58]. Syntectonic sediments have been delivered to the adjacent contractional basins (e.g., Nangqian, Gonjo and Jianchuan basins) [46,59,60] and the marginal seas [61] in response to early-Cenozoic orogenesis (Fig. 4).

Tectonic and topographic inheritance of the Tibetan Plateau

The southwestward younging formation of low-relief plateau surfaces in eastern Tibet documented here provides new insights into the growth of the Tibetan Plateau, as it shows that high topography in eastern Tibet has experienced punctuated development during multiple stages of crustal shortening and thickening from inter-continental terrane accretion and collision to intra-continental tectonism (Figs. 4 and 5). In the Songpan-Garze-Yidun terranes, large tracts of the plateau surfaces have been established prior to the India-Asia collision[20-22,54]. The mountainous landscape in these terranes in eastern Tibet likely emerged much earlier, during the Late-Triassic Indosinian orogeny, coeval with the closure of the Paleo-Tethys Ocean, leading to surface uplift at 2,600 m ± 300 m [62] related to crustal thickening [62,63] (Fig. 4C). If the surface erosion at rates of 0.02-0.09 mm/yr (Table S3) is taken into account, the most conservative estimate of <600 m of eroded rocks during the Cenozoic implies that at least an additional 3,400-3,800 m of post-Late Triassic surface uplift was required under further crustal thickening evidenced by Early Cretaceous and Late Cretaceous-early Cenozoic crustal imbrication in the Longmen Shan fold-and-thrust belt [64-66], rapid cooling on the southern margin of the Litang plateau [67], and flat plateau surfaces recorded by thermochronological peak ages (Fig. 4C). The high topography that we termed "relict plateau" (Fig. 5A), akin to the current one, was apparently reached as a consequence of multi-phased intra-continental mountain building processes that are mostly expressed by crustal shortening and thickening [62-64,66] until early Cenozoic stabilization of low-relief plateau surfaces in the terrane interiors (Figs. 4C, 5B and 5C). In contrast, the sharp topographic gradient (e.g., Longmen-Yulong Mts.) that is mostly localized on the eastern and southeastern margins of the terranes is associated with reactivation of preexisting structural weakness during middle-late Cenozoic times [39,40,63,68] (Fig. 5D).

In comparison with the Songpan-Garze-Yidun terranes, the landscape history of the Qiangtang terrane commenced since the Lhasa-Qiangtang collision in the Cretaceous as reflected by rapid exhumation (Refs.[45,46] and this study), which probably induced moderate surface uplift as reported in central Tibet [54]. Upon the preexisting crustal architecture and paleo-landscape, further topographic growth was likely linked to widespread crustal thickening in the Qiangtang terrane of eastern Tibet in the aftermath of the India-Asia collision (Figs. 4B and 5C), which is attested by intense activity of fold-and-thrust belts in the terrane [46,59,60]. This is supported by paleoaltimetry-based paleoelevations of ~3-3.8 km by late Eocene in the hinterland [34-36]. Such elevated plateaus could be considered as representing the eastward continuation of an incipient plateau in the interior of central Tibet by the late Cretaceous-Eocene [20,54] (Figs. 5A and 5B). The similarity of slow erosion on the low-relief landscape in the Markam-Weixi plateaus (this study), central Tibet [16,20] and the western Himalaya [17] since the late Eocene supports the existence of a single flat, high plateau in the Qiangtang-northern Lhasa terranes, which shares common histories and has been tectonically stable throughout most of the Cenozoic. Plateau uplift expanded to encompass most of central, southern and eastern Tibet along the southern Lhasa terrane by Eocene times (Figs. 4B and 5C), consistent with previous hypotheses for emergence of a "proto-Tibetan Plateau" in central Tibet [4,20,21,54]. Surface uplift of the Zuogong plateau relative to the Markam plateau could be ascribed to reactivated transpression of the Lancangjiang fault during the early Miocene, which concurred with transpressional exhumation and uplift of southern portion of the fault zone [69]. Miocene landscapes in the Zuogong plateau and eastern Lhasa plateau at higher elevations were likely inherited from the late Eocene embryonic plateau in the Qiangtang terrane related to block extrusion [4,124,124,124,12] during northward subduction and translation of the Indian plate [70]. The overlap of thermochronology data from the plateau surface with those from low-elevation valleys (Fig. 1C and 1D) suggests an evolving landscape in the eastern Lhasa terrane, modulated by complex interactions between tectonics and surface erosion [56].

Overall, we stress that preexisting structures and paleo-topography built during Mesozoic-early Cenozoic accretion and collisional orogenesis linked to suturing of the Paleo-, Meso- and Neo-Tethys Oceans set the stage for the latest events of plateau growth in the aftermath of the India-Asia collision. The subsequent growth of eastern Tibet would have been more modest than initially thought since the late Eocene [37].[420,2115] In our model, the physiography of central and eastern Tibetan plateau was grossly achieved before the Indian continent docked into Eurasia (Figs. 4 and 5). Neo-tectonic activities would afterwards only reactivate the outermost preexisting structures of the plateaus. Lower crustal channel flow would passively serve to re-equilibrate further surface uplift and smoothen the topography to its current stage, partly erasing the old, piecemeal topography constituted of discrete plateaus. This view contradicts previous hypotheses in which the plateau mostly developed either in a northward stepwise [4] or outward-growth [20,21] manner during the Cenozoic, or through eastward expansion since the late Miocene [15].

Neogene dismemberment of low-relief plateau surfaces in eastern Tibet

Diachronous formation of the flat plateau surfaces in eastern Tibet contrasts sharply in timing and erosion rates with the high-relief regions of deep river gorges and surface scarps produced by river incision and Neogene-Quaternary tectonic activity, respectively (Fig. 3). Samples from high-elevation (>4,000 m) and low-relief (<600 m) regions of the plateau surfaces yield slow erosion rates of <0.05 mm/yr since topographic stabilization, in contrast to Neogene cooling ages from localities at lower elevations (<4,000 m) with higher relief (>600 m), which record an order of magnitude higher erosion rates of >0.5 mm/yr (Fig. 3B). This bimodal pattern can be explained by decoupling the formation of plateau surfaces from neo-tectonic activity and river incision. In this sense, the stabilization of plateau surfaces mostly predates the onset of incision of large rivers, supportive of river entrenchment into an elevated, preexisting flat landscape [9]. These new results thus refute the paradigm that relates the onset of accelerated river incision to a single episode of surface uplift in eastern Tibet [15,28]. The utility of river incision as a proxy for plateau development linked to lower crustal flow has been called into question previously [9,19,30]. In our interpretation, incision would be mostly indicative of the late stage of crustal channel flow, and not representative of the main development stage of the plateau. Our results also contradict the simulated results for dynamic formation of low-relief relict surfaces [11] as extremely low exhumation rates for the plateau surfaces in the Songpan-Garze-Yidun and eastern Qiangtang terranes preclude prominent tectonic disruption from major river reorganization during most of the Cenozoic. Alternatively, we propose that the separated flat landscapes in eastern Tibet are in fact the remnants of widespread plateau surfaces of different formation ages in each terrane and have been dismembered by rivers and tectonics in Neogene times. The river divides between the Jinsha, Lancang and Nu Rivers exemplify plateau surfaces that experienced intense river incision and faulting during the late Cenozoic [55]. The high-elevation, low-relief landscape in eastern Tibet has been constructed during multiple mountain building processes but is slowly being destructed by a surface river network responding to tectonic activity in the latest stage of the evolution history of the Tibetan Plateau.

Materials and Methods

Methodology of zircon U-Pb geochronology and low-temperature thermochronology

Zircon and apatite grains were separated from rock samples using standard magnetic and heavy liquid separation techniques. In order to quantify complete cooling histories of the rocks, we performed geochronological and thermochronological dating techniques, including zircon U-Pb, zircon (U-Th)/He (ZHe), apatite fission track (AFT) and apatite (U-Th)/He (AHe). The protocols of each dating method are introduced below.

Zircon U-Pb geochronology: Zircon U-Pb geochronological analyses were conducted at China University of Geosciences, Wuhan, China. U-Pb dating was performed using an Agilent 7500a ICP-MS, which is equipped with a GeoLas 2005 excimer laser ablation system at a spot diameter of 32 µm. Zircon 91500 was used as an external standard and analyzed twice every 5 unknowns. To assess age reproducibility and instrument stability, four GJ-1 zircon standards were inserted at the beginning and end of each run. Typical operating conditions and detailed analytical procedures are described in ref.[71]. Selection and integration of analytic signals, time-drift correction, and quantitative calibration for U-Pb dating were performed by ICP-MS DataCal. Ages were accepted with up to 10% and 20% discordance for plutonic and volcanic samples, respectively. The results reported here are $^{206}Pb/^{238}U$ ages for zircon ages $\leq$1.0 Ga. Age-distribution plots and age-concordia diagrams were generated using Isoplot/Ex. ver. 3.75[72].

Apatite fission track: Apatite aliquots were mounted in epoxy, polished and etched for 20 s in a 5.5 M HNO_3 solution at 21 °C. All apatite samples were dated by the external detector method, using uranium-poor muscovite sheets as external detectors. Apatite samples were irradiated at the well-thermalized FRM II Research Reactor of the Technical University Munich, Germany, together with Fish Canyon Tuff and Durango age standards and IRMM540R dosimeter glasses, for a nominal fluence of 4.5×10^{15} neutron cm^{-2}. After irradiation, mica detectors were etched in 48% HF for 18 minutes at 20 °C. In order to increase the number of tracks available for length measurements, replicable mounts of each sample were sent for ^{252}Cffission-fragment irradiation in a nominal vacuum at Melbourne University, Australia. Fission-track analyses were performed at the fission-track laboratory of the Institut des Sciences de la Terre (*ISTerre*) in Grenoble, France, using an Olympus BX51 microscope (1600×, dry) and the FTStage 4.04 system. In general, at least 20 grains were analyzed per sample. Fission-track ages were determined using the ξ-calibration approach and are reported as central ages with $\pm 2\sigma$ errors (95% confidence interval).

Zircon and apatite (U-Th)/He: Zircon and Apatite (U-Th)/He dating was accomplished at the University of Arizona, USA. Normally, 3-5 euhedral zircon and apatite crystals without visible inclusions, fracture and stainless surface were chosen using a stereo-zoom polarized microscope. The geometry of each grain was measured and photographed. Grains larger than 60 μm in both length and width but smaller than 500 μm were accepted for (U-Th)/He analysis. Zircon and apatite grains were wrapped into Nb foil tubes and degassed by laser heating, and then analyzed for He using ^{3}He isotope dilution, cryogenic purification and quadrupole mass spectrometry. The U, Th and Sm concentrations of dissolved aliquots were measured on a sector inductively coupled plasma mass spectrometer. (U-Th)/He ages were processed by applying the α-ejection correction factor [73]. Standard Fish Canyon Tuff zircon and Durango apatite fragments were identically analyzed together with unknowns to validate age determination, age reproducibility and measurement accuracy. Mean ages of each sample were calculated based on all grain ages and relevant errors.

Inverse modeling

The thermal histories of the rocks sampled from the low-relief surfaces of the Zuogong plateau (ZGP), Markam plateau (MKP) and Weixi plateau (WP) were reconstructed utilizing the QTQt inverse modeling code, which allows inferring thermal histories from multiple samples including different thermochronologic systems. The models consider not only the AFT data including ages, track length distributions and kinetic parameters, but also single-grain AHe ages, apatite crystal dimensions and U, Th and Sm concentrations (Datasets S1-S4). See detailed model input in Table S2.

Author Contributions

K.C. conceived the idea. K.C., G.C.W., A.R. and P.v.d.B. conducted the field work. K.C., Y.T.T., P.P., M.B. and T.Y.S. performed the thermochronological analysis and inverse modeling. K.C., A.R., L.H., M.B. and P.v.d.B. wrote the manuscript. All authors discussed and commented on the manuscript.

Data availability: All context and data for evaluation of the conclusions in the paper are present in the paper and/or the supplementary materials. Correspondence and requests for materials should be addressed to K.C. (kai.cao@cug.edu.cn).

Acknowledgments

We thank Paul Kapp for inspiring discussion. We are grateful to Uttam Chowdhury for help in the (U-Th)/He lab at University of Arizona. This study was funded by the National Natural Science Foundation of China (Nos. 91755213, 41672195, 41972223, 41202144), the China Geological Survey (No. DD20190370), China Scholarship Council (No. 201606415003) and the 111 project of China (No. BP0820004). The authors declare that they have no competing interests. All context and data for evaluation of the conclusions in the paper are present in the paper and/or the supplements.

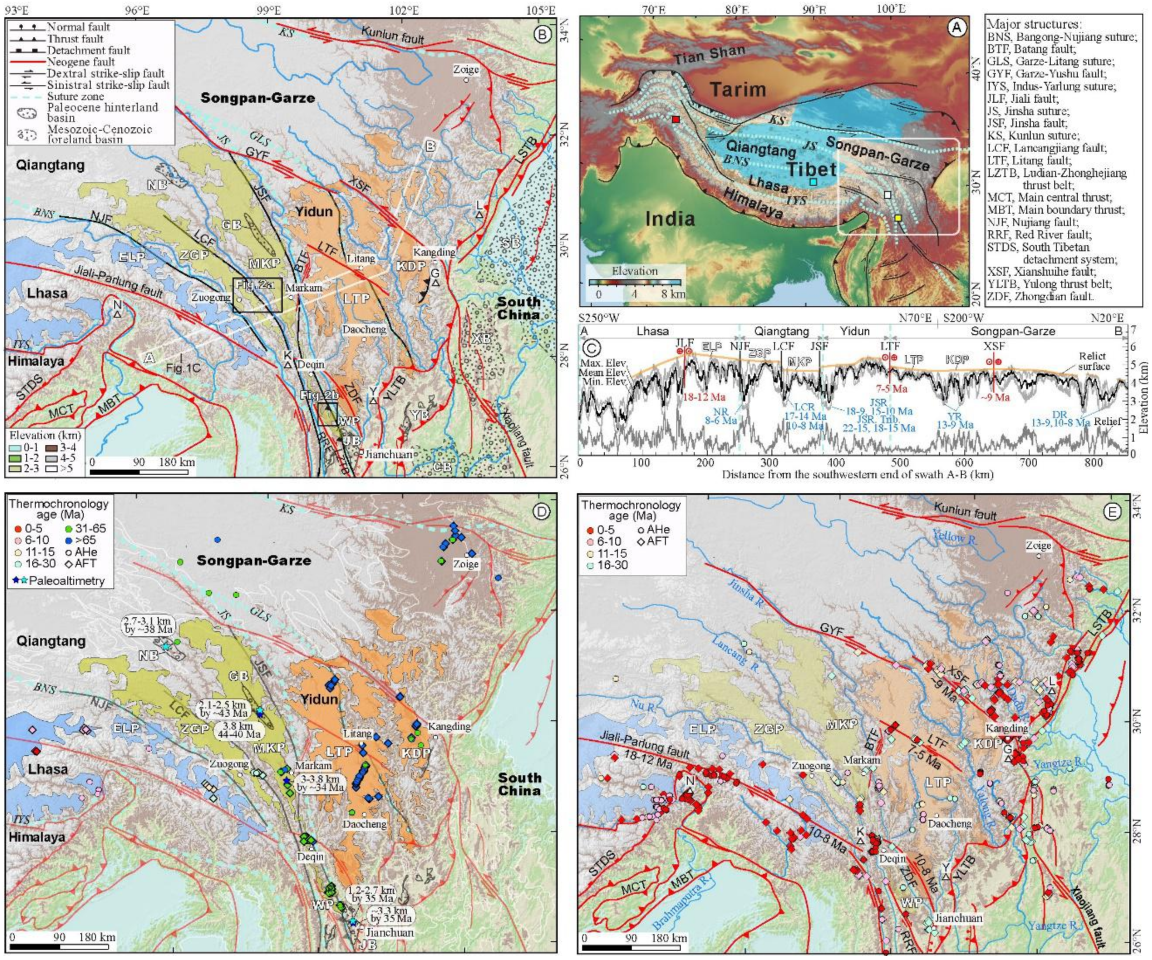

Fig. 1. Topography, tectonics, paleoaltimetry and thermochronology of eastern and southeastern Tibet. (A) Topography of the Tibetan Plateau and adjacent area, with superimposed suture zones, major Cenozoic faults and major rivers. Formation of high-elevation low-relief surfaces by the Eocene, as derived from low-temperature thermochronology in western [17], central [20], eastern and southeastern Tibet (this study) are indicated by red, light blue, white and yellow rectangles, respectively. (B) Map showing main tectonic units, major Cenozoic structures and externally draining rivers. The relict plateau surfaces in different tectonic units are highlighted with color: the eastern Lhasa plateau (ELP) in the Lhasa terrane in light blue, Zuogong plateau (ZGP) and Markam-Weixi plateaus (MKP-WP) in the Qiangtang terrane in yellow, Litang-Kangding plateaus (LTP-KDP) in the Songpan-Garze-Yidun terranes in pink. White box indicates location of topographic swath profile shown in Fig. 1C. (C) Widespread low-relief plateau surfaces in eastern Tibet (colored and outlined after refs.[8,9]; AHe and AFT ages from the high-elevation low-relief plateau surfaces (see the original data in Dataset S5). Paleoelevation reconstruction in the eastern and southeastern Tibet: blue stars show close-to-modern paleoelevations of 3.0-3.8 km [34,35], 3.8 km [36] and 3.3 km [19,34] at Markam, Gonjo (GB) and Jianchuan (JB) basins derived from stable isotopes of volcanic clasts, fossil-leaf assemblages and carbonates by the late Eocene, while light blue stars show moderately high

paleo-elevations of 2.7-3.1 km [37], 2.1-2.5 km (44) and 1.2-2.7 km [24,38] in the Nangqian (NB), Gonjo (GB) and Jianchuan basins, respectively, during the late Eocene. (D) AHe and AFT ages associated with Neogene tectonics and river incision (see the original data in Dataset S5). (E) Topographic swath profile from the Lhasa to Songpan-Garze terranes, across the ELP, ZGP, MKP, LTP and GZP. Brown lines show envelopes of maximum elevations for the highlighted plateau surfaces. Onset timing for river incision and Neogene faults (see Table S1). Abbreviations for basins: CB, Chuxiong basin; GB, Gonjo basin; NB, Nangqian basin; SB, Sichuan basin; XB, Xichang basin; YB, Yanyuan basin. Abbreviations for mountains, peaks and rivers: DR, Dadu River; G, Gongga; L, Longmen Shan; LCR, Lancang River; N, Namche Barwa; NR, Nu River; JR, Jinsha River; K, Kawagebo; Y, Yulong; YR, Yulong River.

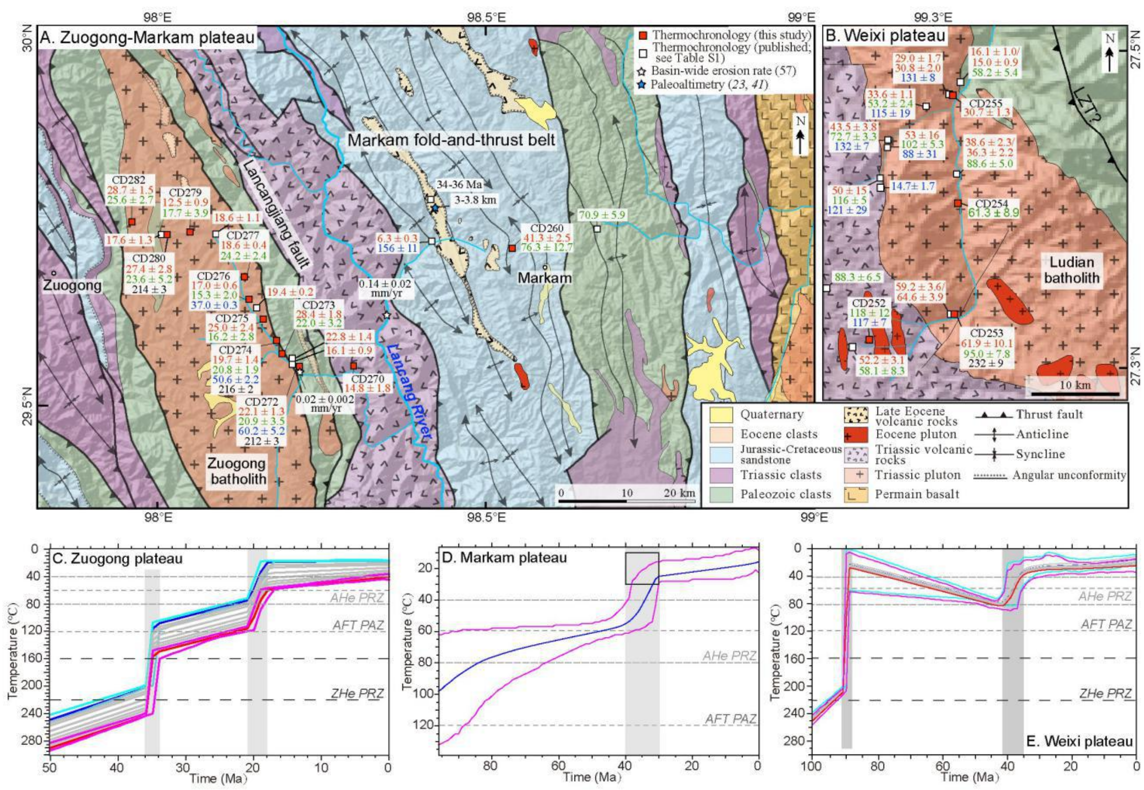

Fig. 2. Simplified geology of the studies areas and cooling histories of selected plateau surfaces. The Zuogong-Markam (A) and Weixi (B) plateaus with geochronological and thermochronological data superimposed on shaded elevation map. Data include zircon U-Pb (black), ZHe (blue), AFT (green) and AHe (red) ages (in Ma, see Table S1 and Datasets S1-5). Cooling histories of the Zuogong (C), Markam (D) and Weixi (E) plateaus in eastern and southeastern Tibet.

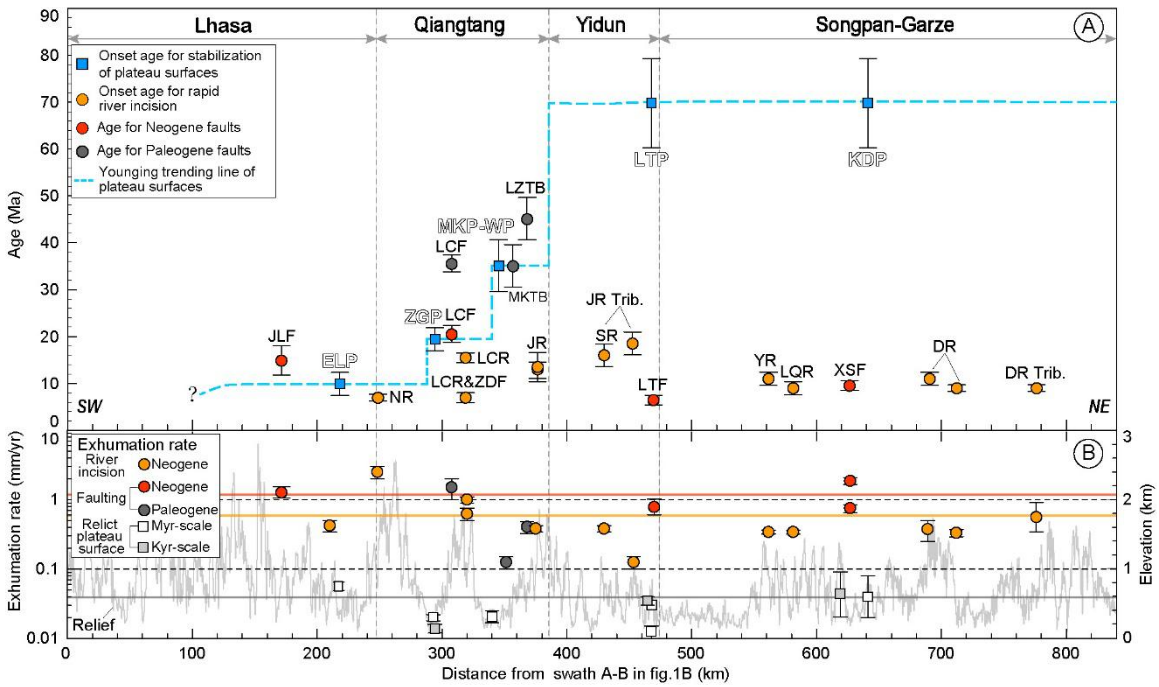

Fig. 3. A synthesis of Cenozoic rapid exhumation and cooling events related to faulting and river incision, as well as formation ages of low-relief landscapes in eastern Tibet. (A) Timing of Neogene tectonic activity and river incision, as well as formation of low-relief plateau surfaces in each terrane. For abbreviations and sources for onset timing of rapid incision of major rivers and faulting, refer to the caption of Fig. 1C. (B) Bimodal pattern of exhumation and erosion rates for stabilized plateau surfaces and areas affected by Neogene tectonics and river incision, correlated with relief across the swath profile A-B in Fig. 1C. The estimated exhumation and erosion rates are derived from the original publications, corresponding to the constraints on the onset of neo-tectonic activity and river incision in Fig. 1C (see details in Table S3). Average exhumation or erosion rates of Cenozoic tectonic activity, Neogene river incision and stabilized plateau surfaces are highlighted by red, orange and gray lines, respectively.

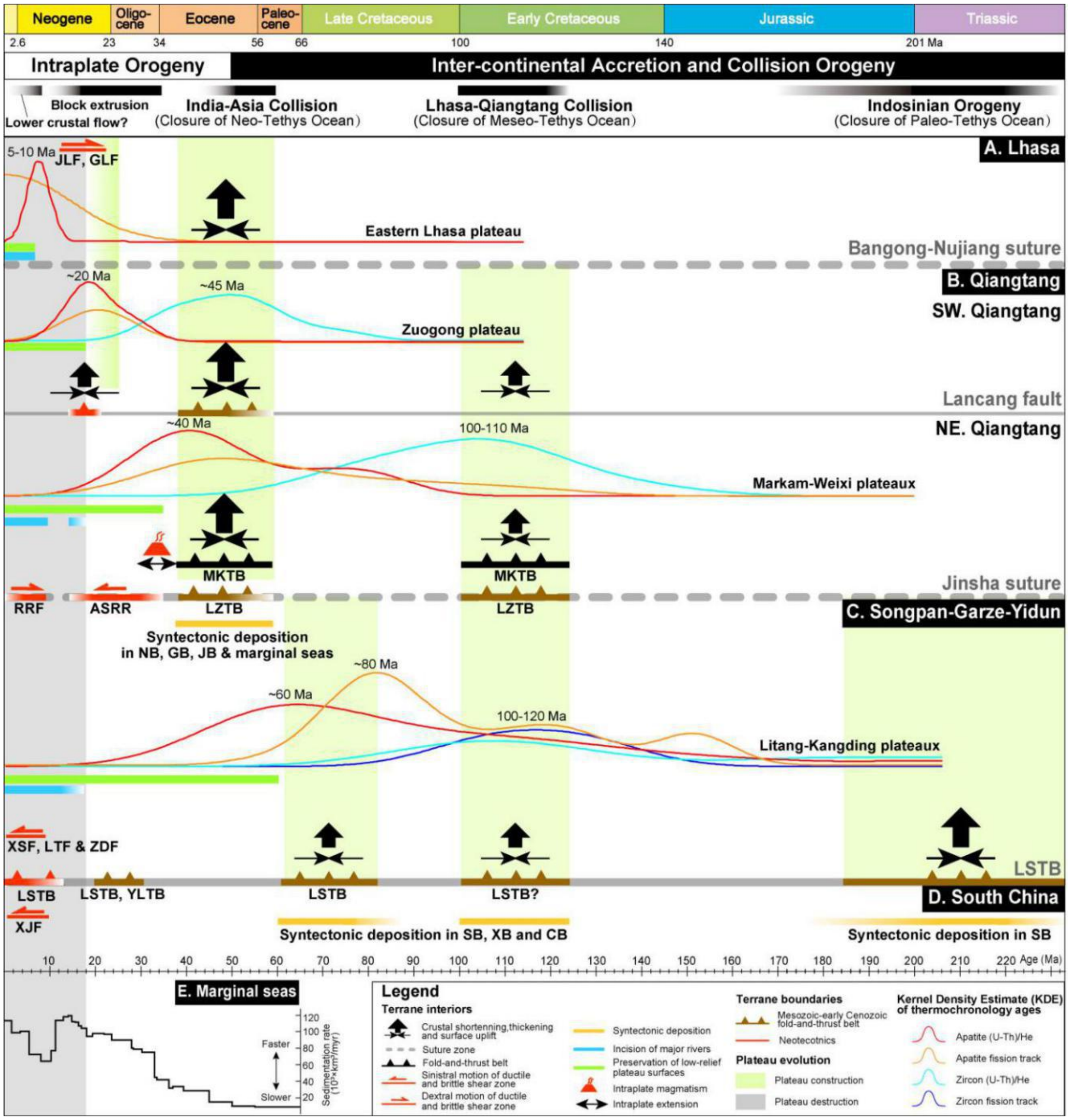

Fig. 4. Comparison of inter- and intra-continental tectonic events, syn-tectonic sedimentation in the hinterland and peripheral basins, and sediment budgets in marginal seas of the southeastern and eastern Asia with development of low-relief plateau surfaces, major river incision and tectonic activity in eastern Tibet. Correlation of regional tectonism, syn-tectonic deposition and thermochronological peak ages for Lhasa (A), Qiangtang (B), Songpan-Garze-Yidun (C) terranes and South China (D) in eastern and southeastern Tibet is used to explain construction and destruction of high-elevation, low-relief plateau surfaces. The peak ages of low temperature thermochronological data are derived from the Kernel density estimate plots by DensityPlotter [74]. (E) Cenozoic sedimentation rate in the marginal seas in southeastern and eastern Asia [75]. For details, see the discussion. Abbreviations as in Fig. 1.

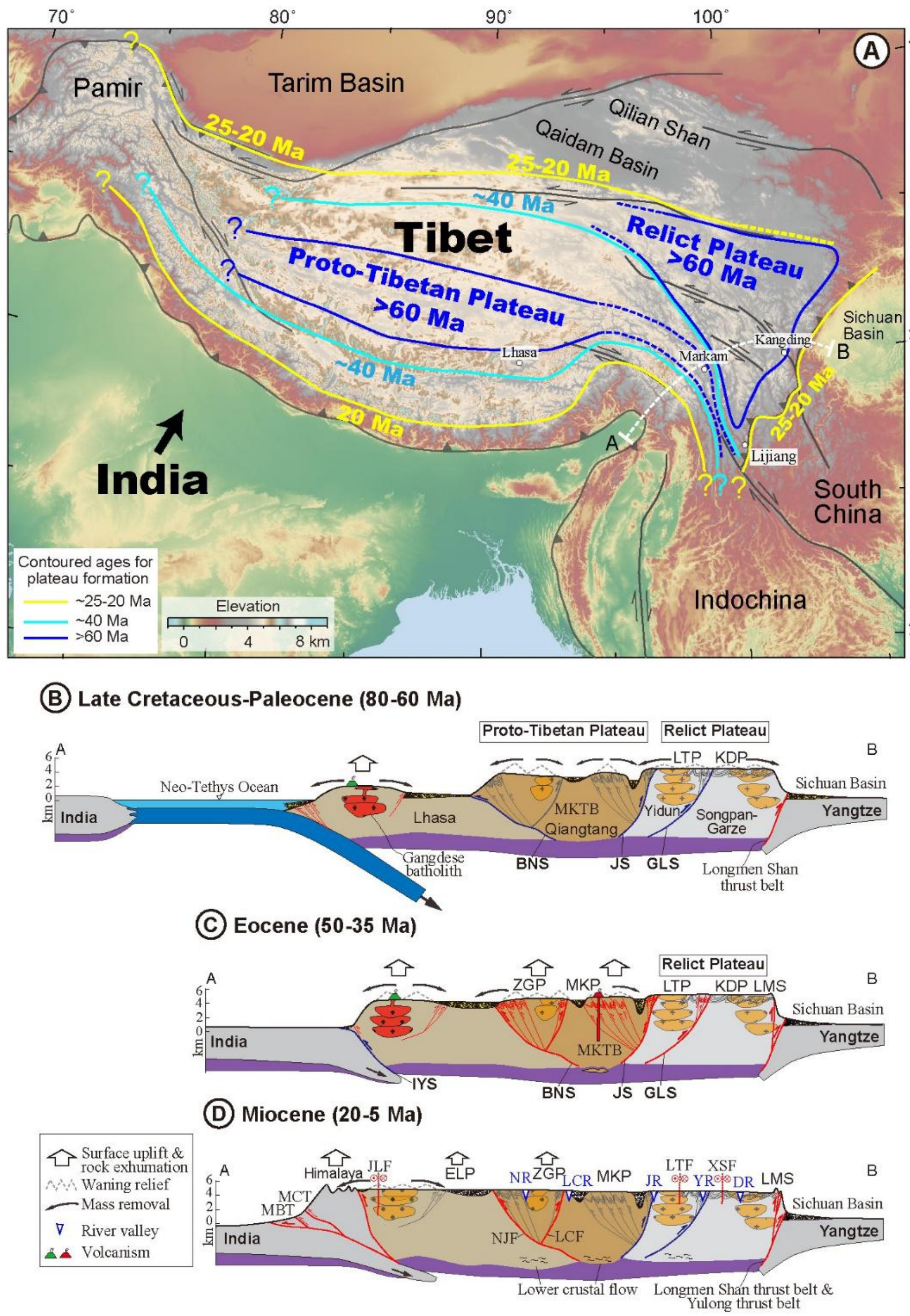

Fig. 5. Proposed model for growth of plateau surfaces inherited from preexisting landscape elements related to multi-phased crustal thickening from inter- to intra-continental orogenesis in the cycles of the Paleo-, Meso- and Neo-Tethys Oceans in eastern Tibet (see a synthesis in Fig. 4). (A) Synthetic age contours of plateau surface formation based on this study and refs. [4,20,21,76]. White curved line delineates the profile of the following cross-sections. (B) Planation of preexisting topographic relief of the proto-Tibetan plateau and relict plateau that have been attained during the Mesozoic orogenesis (see Fig. 4 for details) in the Songpan-Garze-Yidun and Qiangtang terranes. (C) Stabilization of the low-relief landscape in the

Songpan-Garze-Yidun terranes with minor erosion and significant surface uplift of the Qiangtang-Lhasa terranes due to crustal shortening and thickening during the India-Asia collision. (D) Stabilization of the low-relief landscape in the northeastern Qiangtang and Songpan-Garze-Yidun terranes with limited tectonic exhumation and erosion and moderate surface uplift of the southwestern Qiangtang-Lhasa terranes synchronous with block extrusion since the Oligo-Miocene. Heating of the thickened crust lead to lower crustal flow that passively uplifted the surfaces until distinct plateau surfaces are leveled, triggering a late stage of river incision and plateau dissection. Gray thrusts and folds are preexisting structures. Gray dashed lines indicate topographic relief lowered by erosion. Abbreviations as in Fig. 1.

References

1. Hu, X. et al. The timing of India-Asia collision onset-Facts, theories, controversies. *Earth-Sci. Rev.* **160**, 264-299 (2016).
2. Najman, Y. et al. Timing of India-Asia collision: Geological, biostratigraphic, and palaeomagnetic constraints. *Journal of Geophysical Research*. **115**, (2010).
3. Royden, L. H. et al. Surface deformation and lower crustal flow in eastern Tibet. *Science*. **276**, 788-790 (1997).
4. Tapponnier, P. et al. Oblique stepwise rise and growth of the Tibet Plateau. *Science*. **294**, 1671-1677 (2001).
5. An, Z. S., Kutzbach, J. E., Prell, W. L. & Porter, S. C. Evolution of Asian monsoons and phased uplift of the Himalaya-Tibetan Plateau since late Miocene times. *Nature*. **411**, 62-66 (2001).
6. Boos, W. R. & Kuang, Z. Dominant control of the South Asian monsoon by orographic insulation versus plateau heating. *Nature*. **463**, 218-222 (2010).
7. Ding, W., Ree, R. H., Spicer, R. A. & Xing, Y. Ancient orogenic and monsoon-driven assembly of the world’s richest temperate alpine flora. *Science*. **369**, 578 (2020).
8. Clark, M. K. et al. Use of a regional, relict landscape to measure vertical deformation of the eastern Tibetan Plateau. *J. Geophys. Res.* **111**, F3002 (2006).
9. Liu-Zeng, J., Tapponnier, P., Gaudemer, Y. & Ding, L. Quantifying landscape differences across the Tibetan plateau: Implications for topographic relief evolution. *Journal of Geophysical Research*. **113**, (2008).
10. Whipple, K. X., DiBiase, R. A., Ouimet, W. B. & Forte, A. M. Preservation or piracy: Diagnosing low-relief, high-elevation surface formation mechanisms. *Geology*. **45**, 91-94 (2017).
11. Yang, R., Willett, S. D. & Goren, L. In situ low-relief landscape formation as a result of river network disruption. *Nature*. **520**, 526 (2015).
12. Tapponnier, P., Peltzer, G., Le Dain, A. Y., Armijo, R. & Cobbold, P. Propagating extrusion tectonics in Asia: New insights from simple experiments with plasticine. *Geology*. **10**, 611 (1982).
13. Clark, M. K. & Royden, L. H. Topographic ooze: Building the eastern margin of Tibet by lower crustal flow. *Geology*. **28**, 703-706 (2000).
14. Han, Z. et al. Internal Drainage Has Sustained Low‐Relief Tibetan Landscapes Since the Early Miocene. *Geophys. Res. Lett.* **46**, 8741-8752 (2019).
15. Clark, M. K. et al. Late Cenozoic uplift of southeastern Tibet. *Geology*. **33**, 525-528 (2005).
16. Hetzel, R. et al. Peneplain formation in southern Tibet predates the India-Asia collision and plateau uplift. *Geology*. **39**, 983-986 (2011).
17. van der Beek, P. et al. Eocene Tibetan plateau remnants preserved in the northwest Himalaya. *Nat. Geosci.* **2**, 364-368 (2009).
18. Ding, L. et al. The Andean-type Gangdese Mountains: Paleoelevation record from the Paleocene–Eocene Linzhou Basin. *Earth Planet. Sc. Lett.* **392**, 250-264 (2014).
19. Hoke, G. D., Liu-Zeng, J., Hren, M. T., Wissink, G. K. & Garzione, C. N. Stable isotopes reveal high southeast Tibetan Plateau margin since the Paleogene. *Earth Planet. Sc. Lett.* **394**, 270-278 (2014).

20. Rohrmann, A. et al. Thermochronologic evidence for plateau formation in central Tibet by 45 Ma. *Geology*. **40**, 187-190 (2012).
21. Wang, C. et al. Constraints on the early uplift history of the Tibetan Plateau. *Proceedings of the National Academy of Sciences*. **105**, 4987-4992 (2008).
22. Kapp, P., DeCelles, P. G., Gehrels, G. E., Heizler, M. & Ding, L. Geological records of the Lhasa-Qiangtang and Indo-Asian collisions in the Nima area of central Tibet. *Geol. Soc. Am. Bull.* **119**, 917-933 (2007).
23. Rowley, D. B. Stable Isotope-Based Paleoaltimetry: Theory and Validation. *Reviews in Mineralogy and Geochemistry*. **66**, 23-52 (2007).
24. Gourbet, L. et al. Reappraisal of the Jianchuan Cenozoic basin stratigraphy and its implications on the SE Tibetan plateau evolution. *Tectonophysics*. **700-701**, 162-179 (2017).
25. Botsyun, S. et al. Revised paleoaltimetry data show low Tibetan Plateau elevation during the Eocene. *Science*. **363**, q1436 (2019).
26. Reiners, P. W. Thermochronologic approaches to paleotopography. *Reviews in Mineralogy and Geochemistry*. **66**, 243-267 (2007).
27. Burchfiel, B. C. & Chen, Z. Tectonics of the southeastern Tibetan Plateau and its adjacent foreland. *Geological Society of America Memoirs*. **210**, 1-164 (2012).
28. Ouimet, W. et al. Regional incision of the eastern margin of the Tibetan Plateau. *Lithosphere-US*. **2**, 50-63 (2010).
29. McPhillips, D. et al. Dating the incision of the Yangtze River gorge at the First Bend using three ‐ nuclide burial ages. *Geophys. Res. Lett.* **43**, 101-110 (2016).
30. Nie, J. et al. Rapid incision of the Mekong River in the middle Miocene linked to monsoonal precipitation. *Nat. Geosci.* **11**, 944-948 (2018).
31. Tian, Y., Kohn, B. P., Hu, S. & Gleadow, A. J. W. Synchronous fluvial response to surface uplift in the eastern Tibetan Plateau: Implications for crustal dynamics. *Geophys. Res. Lett.* **42**, 29-35 (2015).
32. Zhang, Y. et al. Cooling history of the Gongga batholith: Implications for the Xianshuihe Fault and Miocene kinematics of SE Tibet. *Earth Planet. Sc. Lett.* **465**, 1-15 (2017).
33. Zhang, Y. et al. Timing and rate of exhumation along the Litang fault system, implication for fault reorganization in Southeast Tibet. *Tectonics*. **34**, 1219-1243 (2015).
34. Li, S., Currie, B. S., Rowley, D. B. & Ingalls, M. Cenozoic paleoaltimetry of the SE margin of the Tibetan Plateau: Constraints on the tectonic evolution of the region. *Earth Planet. Sc. Lett.* **432**, 415-424 (2015).
35. Su, T. et al. Uplift, climate and biotic changes at the Eocene – Oligocene transition in south-eastern Tibet. *National Science Review*, 1-10 (2018).
36. Xiong, Z. et al. The early Eocene rise of the Gonjo Basin, SE Tibet: From low desert to high forest. *Earth Planet. Sc. Lett.* **543**, 116312 (2020).
37. Li, L. et al. Carbonate stable and clumped isotopic evidence for late Eocene moderate to high elevation of the east-central Tibetan Plateau and its geodynamic implications. *GSA Bulletin*. **131**, 831-844 (2018).
38. Wu, J. et al. Paleoelevations in the Jianchuan Basin of the southeastern Tibetan Plateau based on stable isotope and pollen grain analyses. *Palaeogeography, Palaeoclimatology, Palaeoecology*. **510**, 93-108 (2018).
39. Cao, K. et al. Oligocene-Early Miocene topographic relief generation of southeastern Tibet triggered by thrusting. *Tectonics*. **38**, 374-391 (2019).
40. Wang, E. et al. Two-phase growth of high topography in eastern Tibet during the Cenozoic. *Nat. Geosci.*, 640-645 (2012).
41. Tian, Y., Kohn, B. P., Gleadow, A. J. W. & Hu, S. Constructing the Longmen Shan eastern Tibetan Plateau margin: Insights from low-temperature thermochronology. *Tectonics*. **32**, 576-592 (2013).
42. Reiners, P. W. & Brandon, M. T. Using thermochronology to understand orogenic erosion. *Annu. Rev. Earth Pl. Sc.* **34**, 419-466 (2006).
43. Xiao, P. et al. The thermal history of the Baimaxueshan pluton in Deqin area and its implications for the tectonic-geomorphic evolution in the Three River Region of Tibetan Plateau. *Acta Petrol.*

Sin. **31**, 1348-1360 (2015).

44. Wilson, C. J. L. & Fowler, A. P. Denudational response to surface uplift in east Tibet: Evidence from apatite fission-track thermochronology. *GSA Bulletin*. **123**, 1966-1987 (2011).

45. Liu-Zeng, J. et al. Multiple episodes of fast exhumation since Cretaceous in southeast Tibet, revealed by low-temperature thermochronology. *Earth Planet. Sc. Lett.* **490**, 62-76 (2018).

46. Cao, K. et al. Thrusting, exhumation, and basin fill on the western margin of the South China block during the India-Asia collision. *GSA Bulletin*, (2020).

47. Yang, R. et al. Spatial and temporal pattern of erosion in the Three Rivers Region, southeastern Tibet. *Earth Planet. Sc. Lett.* **433**, 10-20 (2016).

48. Henck, A. C., Huntington, K. W., Stone, J. O., Montgomery, D. R. & Hallet, B. Spatial controls on erosion in the Three Rivers Region, southeastern Tibet and southwestern China. *Earth Planet. Sc. Lett.* **303**, 71-83 (2011).

49. Fu, P. et al. Ice cap erosion patterns from bedrock 10Be and 26Al, southeastern Tibetan Plateau. *Earth Surf. Proc. Land.* **44**, 918-932 (2018).

50. Ouimet, W. B., Whipple, K. X. & Granger, D. E. Beyond threshold hillslopes: Channel adjustment to base-level fall in tectonically active mountain ranges. *Geology*. **37**, 579-582 (2009).

51. Tian, Y., Kohn, B. P., Gleadow, A. J. W. & Hu, S. A thermochronological perspective on the morphotectonic evolution of the southeastern Tibetan Plateau. *Journal of Geophysical Research: Solid Earth*. **119**, 2013J-10429J (2014).

52. Xu, G. & Kamp, P. J. J. Tectonics and denudation adjacent to the Xianshuihe Fault, eastern Tibetan Plateau: Constraints from fission track thermochronology. *J. Geophys. Res.* **105**, 19231-19251 (2000).

53. Zhang, H. et al. Pulsed exhumation of interior eastern Tibet: Implications for relief generation mechanisms and the origin of high-elevation planation surfaces. *Earth Planet. Sc. Lett.* **449**, 176-185 (2016).

54. Kapp, P. & DeCelles, P. G. Mesozoic – Cenozoic geological evolution of the Himalayan-Tibetan orogen and working tectonic hypotheses. *Am. J. Sci.* **319**, 159-254 (2019).

55. Replumaz, A. et al. Tectonic Control on Rapid Late - Miocene – Quaternary incision of the Mekong River knickzone, Southeast Tibetan Plateau. *Tectonics*. **39**, e2019T-e5782T (2020).

56. Zeitler, P. K. et al. Tectonics and topographic evolution of Namche Barwa and the easternmost Lhasa block, Tibet. In: Nie, J., Horton, B. K. & Hoke, G. D., editors. *Toward an Improved Understanding of Uplift Mechanisms and the Elevation History of the Tibetan Plateau*: Geological Society of America; 2014. p. 0.

57. Montgomery, D. R. & Brandon, M. T. Topographic controls on erosion rates in tectonically active mountain ranges. *Earth Planet. Sc. Lett.* **201**, 481-489 (2002).

58. Deng, B. et al. Heavy mineral analysis and detrital U-Pb ages of the intracontinental Paleo-Yangzte basin: Implications for a transcontinental source-to-sink system during Late Cretaceous time. *GSA Bulletin*. **130**, 2087-2109 (2018).

59. Horton, B. K., Yin, A., Spurlin, M. S., Zhou, J. & Wang, J. Paleocene – Eocene syncontractional sedimentation in narrow, lacustrine-dominated basins of east-central Tibet. *Geol. Soc. Am. Bull.* **114**, 771-786 (2002).

60. Studnicki-Gizbert, C., Burchfiel, B. C., Li, Z. & Chen, Z. Early Tertiary Gonjo basin, eastern Tibet: Sedimentary and structural record of the early history of India-Asia collision. *Geosphere*. **4**, 713-735 (2008).

61. Clift, P. D. et al. A Late Eocene - Oligocene Through - Flowing River Between the Upper Yangtze and South China Sea. *Geochemistry, geophysics, geosystems : G3*. **21**, n/a-n/a (2020).

62. Zhan, Q. et al. Constructing the Eastern Margin of the Tibetan Plateau During the Late Triassic. *Journal of Geophysical Research: Solid Earth*. **123**, 10, 410-449, 459 (2018).

63. Roger, F., Jolivet, M., Cattin, R. & Malavieille, J. Mesozoic-Cenozoic tectonothermal evolution of the eastern part of the Tibetan Plateau (Songpan-Garzê, Longmen Shan area): insights from thermochronological data and simple thermal modelling. *Geological Society, London, Special Publications*. **353**, 9 (2011).

64. Tian, Y. et al. Late Cretaceous – earliest Paleogene deformation in the Longmen Shan fold-and-thrust belt, eastern Tibetan Plateau margin: Pre-Cenozoic thickened crust? *Tectonics*. **35**, 2293-

2312 (2016).

65. Zhou, M., Yan, D., Vasconcelos, P. M., Li, J. & Hu, R. Structural and geochronological constraints on the tectono-thermal evolution of the Danba domal terrane, eastern margin of the Tibetan plateau. *J. Asian Earth Sci.* **33**, 414-427 (2008).

66. Yan, D., Zhou, M., Li, S. & Wei, G. Structural and geochronological constraints on the Mesozoic-Cenozoic tectonic evolution of the Longmen Shan thrust belt, eastern Tibetan Plateau. *Tectonics*. **30**, n/a-n/a (2011).

67. Gourbet, L. et al. Evolution of the Yangtze River network, southeastern Tibet: Insights from thermochronology and sedimentology. *Lithosphere-US*. **12**, 3-18 (2019).

68. Kirby, E. et al. Late Cenozoic evolution of the eastern margin of the Tibetan Plateau: Inferences from $^{40}Ar/^{39}Ar$ and (U-Th)/He thermochronology. *Tectonics*. **21**, 1001 (2002).

69. Zhang, B. et al. The Biluoxueshan transpressive deformation zone monitored by synkinematic plutons, around the Eastern Himalayan Syntaxis. *Tectonophysics*. **574-575**, 158-180 (2012).

70. Replumaz, A., Capitanio, F. A., Guillot, S., Negredo, A. M. & Villaseñor, A. The coupling of Indian subduction and Asian continental tectonics. *Gondwana Res.* **26**, 608-626 (2014).

71. Liu, Y. et al. In situ analysis of major and trace elements of anhydrous minerals by LA-ICP-MS without applying an internal standard. *Chem. Geol.* **257**, 34-43 (2008).

72. Ludwig, K. R. *User's Manual for Isoplot 3.75: A geochronological toolkit for microsoft excel*. (Berkeley Geochronology Center Special Publication No. 5, Berkeley, California, 2012).

73. Farley, K. A. (U-Th)/He Dating: Techniques, Calibrations, and Applications. *Reviews in Mineralogy and Geochemistry*. **47**, 819-844 (2002).

74. Vermeesch, P. On the visualisation of detrital age distributions. *Chem. Geol.* **312-313**, 190-194 (2012).

75. Clift, P. D. Controls on the erosion of Cenozoic Asia and the flux of clastic sediment to the ocean. *Earth Planet. Sc. Lett.* **241**, 571-580 (2006).

76. Cao, K., Wang, G., Bernet, M., van der Beek, P. & Zhang, K. Exhumation history of the West Kunlun Mountains, northwestern Tibet: Evidence for a long-lived, rejuvenated orogen. *Earth Planet. Sc. Lett.* **432**, 391-403 (2015).

Figures

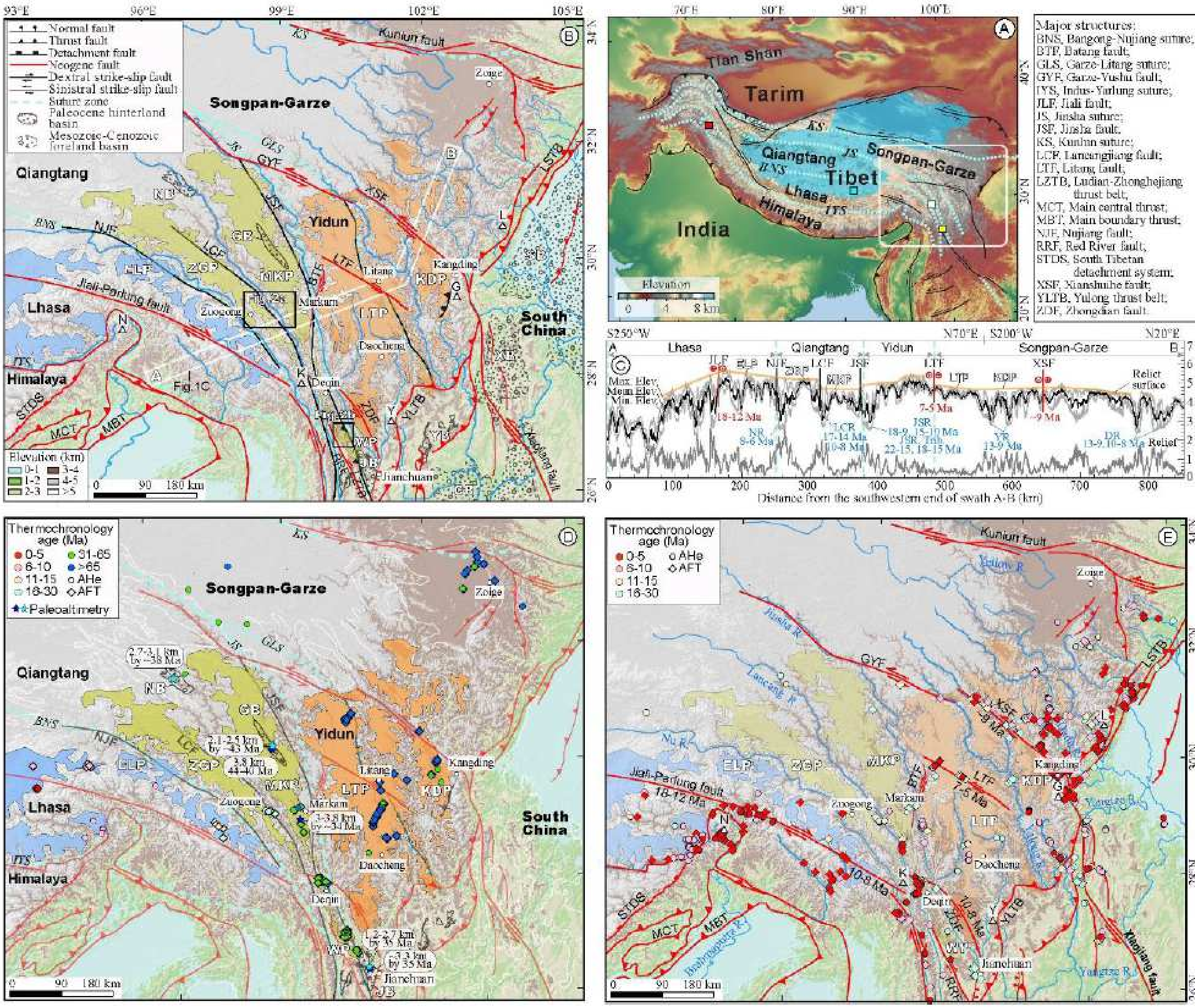

Figure 1

Topography, tectonics, paleoaltimetry and thermochronology of eastern and southeastern Tibet. (A) Topography of the Tibetan Plateau and adjacent area, with superimposed suture zones, major Cenozoic faults and major rivers. Formation of high-elevation low-relief surfaces by the Eocene, as derived from low-temperature thermochronology in western 17, central 20, eastern and southeastern Tibet (this study) are indicated by red, light blue, white and yellow rectangles, respectively. (B) Map showing main tectonic units, major Cenozoic structures and externally draining rivers. The relict plateau surfaces in different tectonic units are highlighted with color: the eastern Lhasa plateau (ELP) in the Lhasa terrane in light blue, Zuogong plateau (ZGP) and Markam-Weixi plateaus (MKP-WP) in the Qiangtang terrane in yellow, Litang-Kangding plateaus (LTP-KDP) in the Songpan-Garze-Yidun terranes in pink. White box indicates location of topographic swath profile shown in Fig. 1C. (C) Widespread low-relief plateau surfaces in eastern Tibet (colored and outlined after refs.8,9; AHe and AFT ages from the high-elevation low-relief plateau surfaces (see the original data in Dataset S5). Paleoelevation reconstruction in the eastern and southeastern Tibet: blue stars show close-to-modern paleoelevations of 3.0-3.8 km 34,35, 3.8 km 36 and 3.3 km 19,34 at Markam, Gonjo (GB) and Jianchuan (JB) basins derived from stable isotopes of volcanic clasts, fossil-leaf assemblages and carbonates by the late Eocene, while light blue stars show moderately high paleo-elevations of 2.7-3.1 km 37, 2.1-2.5 km (44) and 1.2-2.7 km 24,38 in the Nangqian (NB), Gonjo (GB) and Jianchuan basins, respectively, during the late Eocene. (D) AHe and AFT ages associated with Neogene tectonics and river incision (see the original data in Dataset S5). (E) Topographic swath profile from the Lhasa to Songpan-Garze terranes, across the ELP, ZGP, MKP, LTP and GZP. Brown lines show envelopes of maximum elevations for the highlighted plateau surfaces. Onset timing for river incision and Neogene faults (see Table S1). Abbreviations for basins: CB, Chuxiong basin; GB, Gonjo basin; NB, Nangqian basin; SB, Sichuan basin; XB, Xichang basin; YB, Yanyuan basin. Abbreviations for mountains, peaks and rivers: DR, Dadu River; G, Gongga; L, Longmen Shan; LCR, Lancang River; N, Namche Barwa; NR, Nu River; JR, Jinsha River; K, Kawagebo; Y, Yulong; YR, Yulong River. Note: The designations employed and the presentation of the material on this map do not imply the expression of any opinion whatsoever on the part of Research Square concerning the legal status of any country, territory, city or area or of its authorities, or concerning the delimitation of its frontiers or boundaries. This map has been provided by the authors.

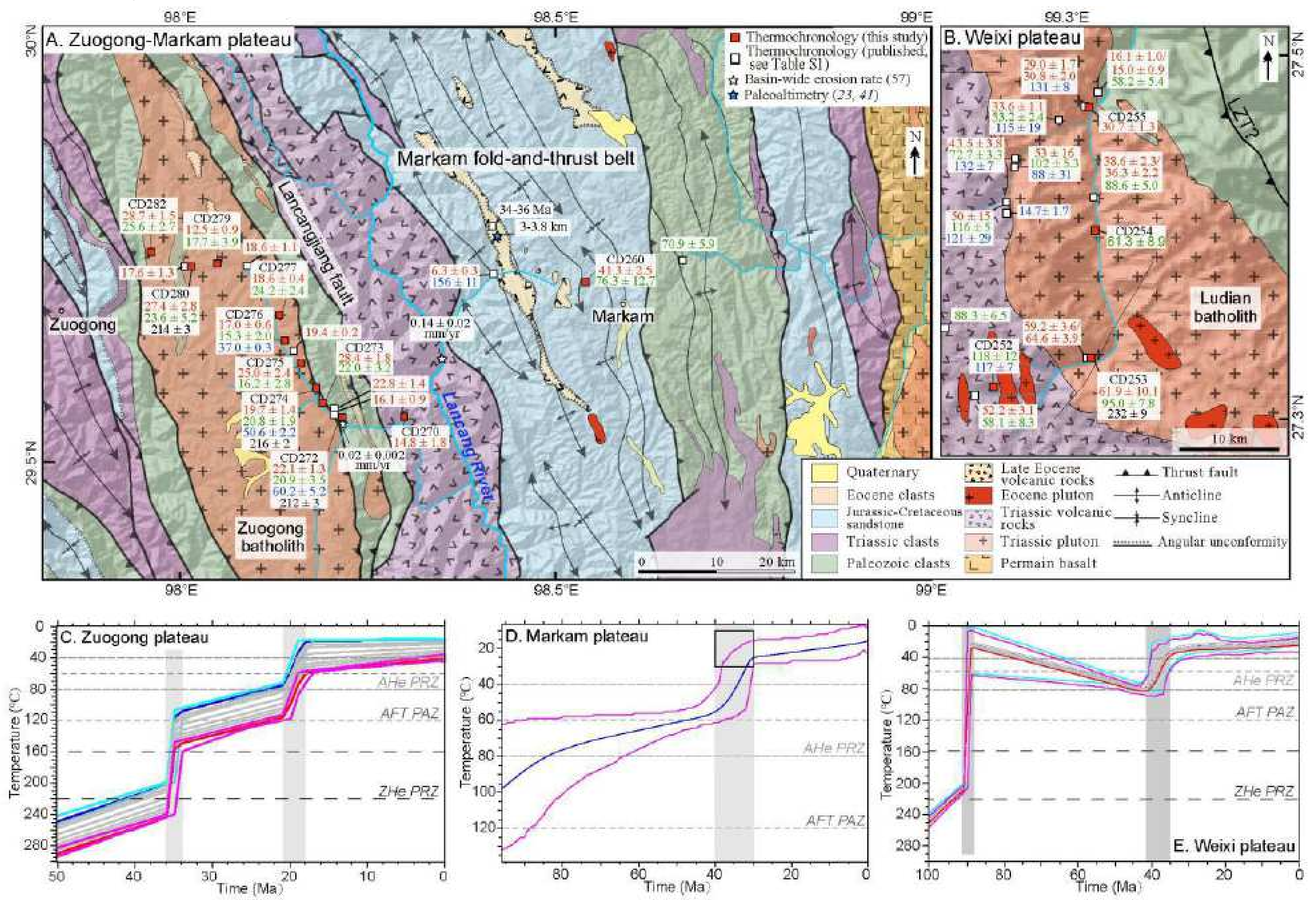

Figure 2

Simplified geology of the studies areas and cooling histories of selected plateau surfaces. The Zuogong-Markam (A) and Weixi (B) plateaus with geochronological and thermochronological data superimposed on shaded elevation map. Data include zircon U-Pb (black), ZHe (blue), AFT (green) and AHe (red) ages (in Ma, see Table S1 and Datasets S1-5). Cooling histories of the Zuogong (C), Markam (D) and Weixi (E) plateaus in eastern and southeastern Tibet. Note: The designations employed and the presentation of the material on this map do not imply the expression of any opinion whatsoever on the part of Research Square concerning the legal status of any country, territory, city or area or of its authorities, or concerning the delimitation of its frontiers or boundaries. This map has been provided by the authors.

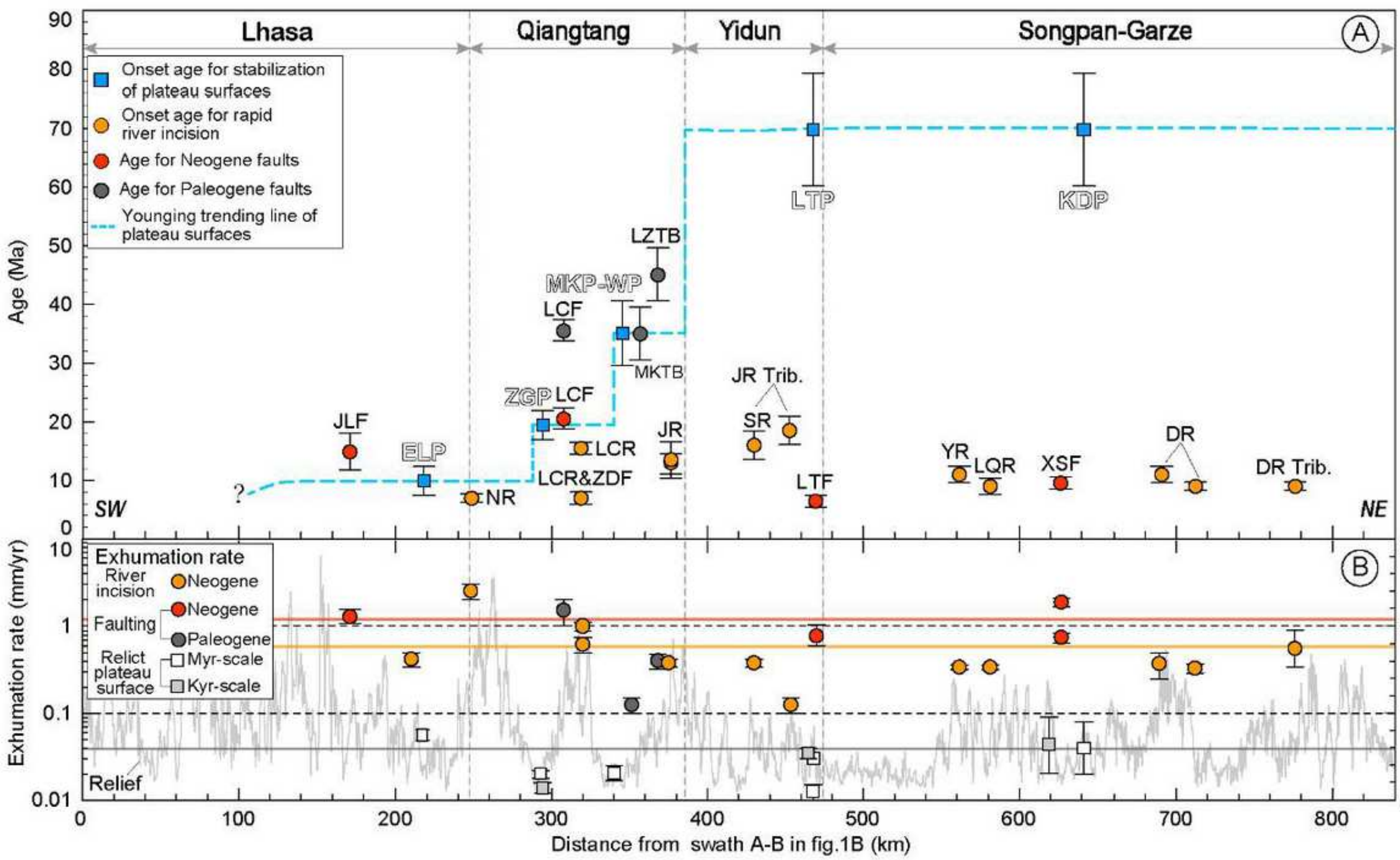

Figure 3

A synthesis of Cenozoic rapid exhumation and cooling events related to faulting and river incision, as well as formation ages of low-relief landscapes in eastern Tibet. (A) Timing of Neogene tectonic activity and river incision, as well as formation of low-relief plateau surfaces in each terrane. For abbreviations and sources for onset timing of rapid incision of major rivers and faulting, refer to the caption of Fig. 1C. (B) Bimodal pattern of exhumation and erosion rates for stabilized plateau surfaces and areas affected by Neogene tectonics and river incision, correlated with relief across the swath profile A-B in Fig. 1C. The estimated exhumation and erosion rates are derived from the original publications, corresponding to the constraints on the onset of neo-tectonic activity and river incision in Fig. 1C (see details in Table S3).

Average exhumation or erosion rates of Cenozoic tectonic activity, Neogene river incision and stabilized plateau surfaces are highlighted by red, orange and gray lines, respectively.

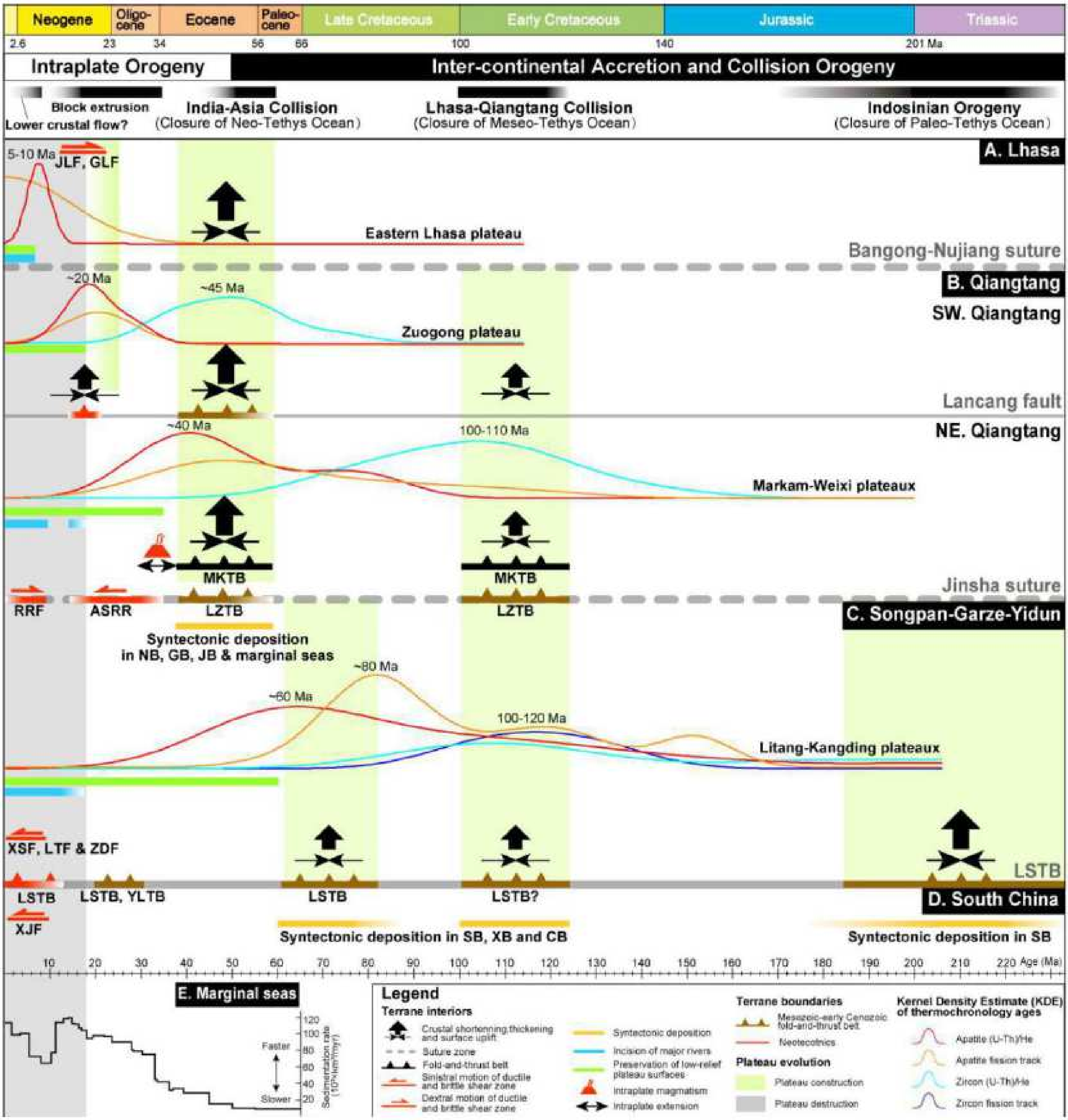

Figure 4

Comparison of inter- and intra-continental tectonic events, syn-tectonic sedimentation in the hinterland and peripheral basins, and sediment budgets in marginal seas of the southeastern and eastern Asia with development of low-relief plateau surfaces, major river incision and tectonic activity in eastern Tibet.

Correlation of regional tectonism, syn-tectonic deposition and thermochronological peak ages for Lhasa (A), Qiangtang (B), Songpan-Garze-Yidun (C) terranes and South China (D) in eastern and southeastern Tibet is used to explain construction and destruction of high-elevation, low-relief plateau surfaces. The peak ages of low temperature thermochronological data are derived from the Kernel density estimate plots by DensityPlotter 74. (E) Cenozoic sedimentation rate in the marginal seas in southeastern and eastern Asia 75. For details, see the discussion. Abbreviations as in Fig. 1.

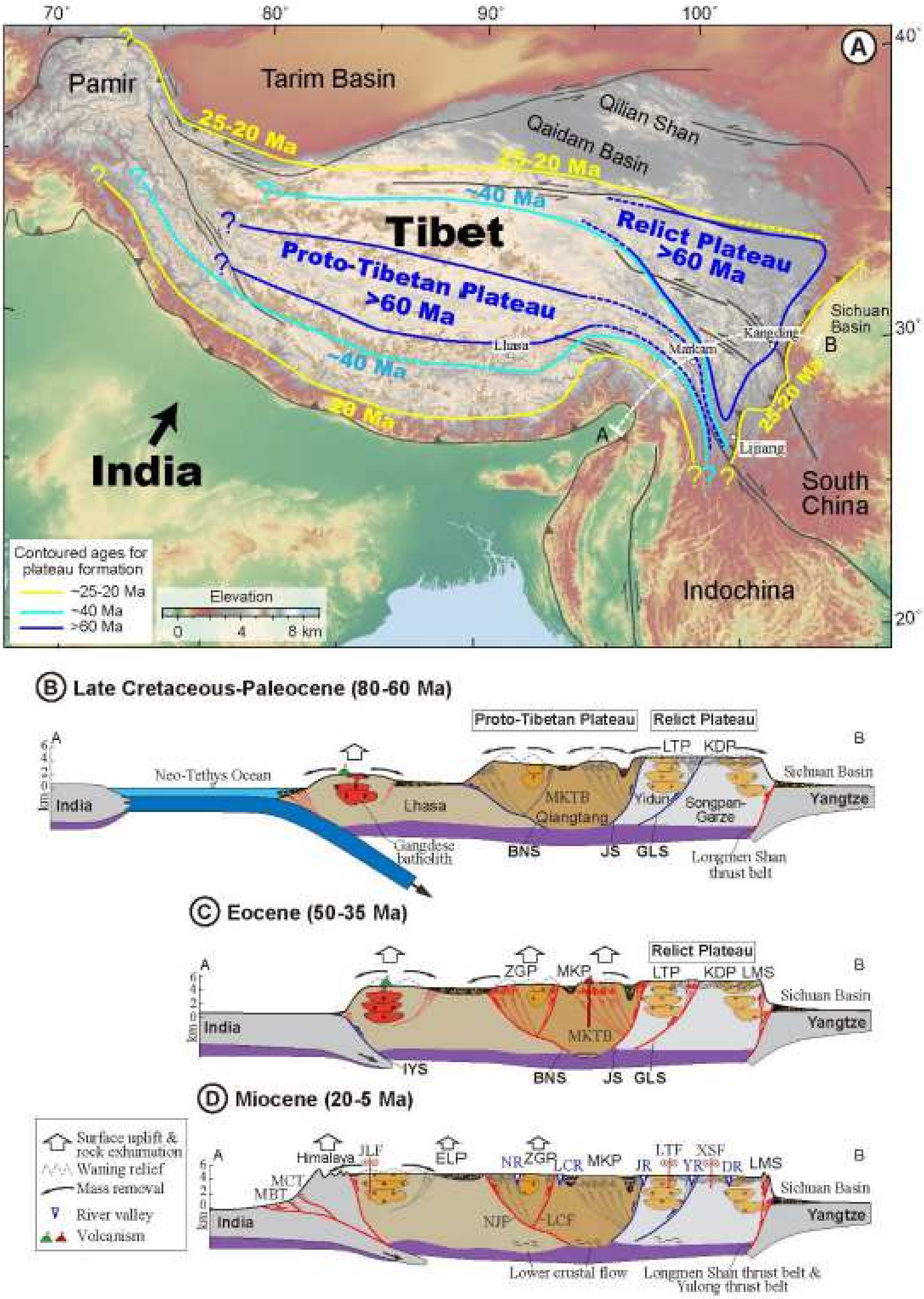

Figure 5

Proposed model for growth of plateau surfaces inherited from preexisting landscape elements related to multi-phased crustal thickening from inter- to intra-continental orogenesis in the cycles of the Paleo-, Meso- and Neo-Tethys Oceans in eastern Tibet (see a synthesis in Fig. 4). (A) Synthetic age contours of plateau surface formation based on this study and refs. 4,20,21,76. White curved line delineates the profile of the following cross-sections. (B) Planation of preexisting topographic relief of the proto-Tibetan plateau and relict plateau that have been attained during the Mesozoic orogenesis (see Fig. 4 for details) in the Songpan-Garze-Yidun and Qiangtang terranes. (C) Stabilization of the low-relief landscape in the Songpan-Garze-Yidun terranes with minor erosion and significant surface uplift of the Qiangtang-Lhasa terranes due to crustal shortening and thickening during the India-Asia collision. (D) Stabilization of the low-relief landscape in the northeastern Qiangtang and Songpan-Garze-Yidun terranes with limited tectonic exhumation and erosion and moderate surface uplift of the southwestern Qiangtang-Lhasa terranes synchronous with block extrusion since the Oligo-Miocene. Heating of the thickened crust lead to lower crustal flow that passively uplifted the surfaces until distinct plateau surfaces are leveled, triggering a late stage of river incision and plateau dissection. Gray thrusts and folds are preexisting structures. Gray dashed lines indicate topographic relief lowered by erosion. Abbreviations as in Fig. 1. Note: The designations employed and the presentation of the material on this map do not imply the expression of any opinion whatsoever on the part of Research Square concerning the legal status of any country, territory, city or area or of its authorities, or concerning the delimitation of its frontiers or boundaries. This map has been provided by the authors.

Supplementary Files

This is a list of supplementary files associated with this preprint. Click to download.

- TableS1Sampleinfo.pdf
- TableS2Thermalhistorymodelinputtable.pdf
- TableS3exhumationrate.pdf
- DatasetS1AFT.xlsx
- DatasetS2AHe.xlsx
- DatasetS3ZHe.xlsx
- DatasetS4UPbdata.xlsx
- DatasetS5Syntheticthermochronologydata.xlsx
- Fig.S1.thermochronology.jpg
- Fig.S2Inversemodeling.jpg